ST-ECF Instrument Science Report ACS 2003-001

The in-orbit wavelength calibration of the WFC G800L grism

A. Pasquali, N. Pirzkal, J.R. Walsh
March 5, 2003

ABSTRACT

We present the G800L grism spectra of the Wolf-Rayet stars WR45 and WR96 acquired with the Wide Field Channel during the Servicing Mission Orbital Verification (SMOV) tests and the early Cycle 11 INTERIM calibration programme. We discuss the procedure for fitting the dispersion correction of the grism. The targets have been observed in ten different positions across the WFC field of view in order to quantify the field dependence of the grism physical properties and wavelength solution. We have obtained for non-drizzled spectra an average dispersion of 39.2 A/pix in 1st order, 20.5 A/pix in 2nd order, 14.1 A/pix in 3rd order, -42.5 A/pix in -1st order, -21.2 A/pix in -2nd order and -13.7 A/pix in -3rd order. The amplitude of the dispersion field dependence is about 11% from the centre to the edges of the field of view; the direction of the field dependence is the diagonal from the image left top corner to the bottom right corner. The same trends are observed for all grism orders. We also describe the calibration files derived from these SMOV and INTERIM data which are used by the ST-ECF extraction package aXe.

Introduction

The Servicing Mission Orbital Verification tests were designed for the WFC and HRC grism according to the spectroscopic simulations of Pasquali et al. (2001). They showed that Wolf-Rayet (WR) stars can fulfil the requirements for wavelength calibration targets, viz:

i) the target brightness allows for reasonably short exposure times;

ii) the target optical spectrum presents a significant number of unresolved emission lines;

iii) no extended nebulosity is associated with the targets which would degrade the spectral resolution of the instrument and increase the local background;
iv) the spectrophotometric variability is negligible;
v) the targets should not lie in crowded fields to avoid contamination by nearby spectra;
vi) the targets should be visible as long as possible to allow repeated HST visits.
Requirement ii) is particularly met by WR stars of spectral type WC6 - WC9. SLIM 1.0 (Pirzkal, Pasquali et al. 2001) simulations showed that WC6-9 stars provide a good sample of lines over the spectral range of the ACS grism (~0.5 to ~1 μm) which allow the wavelength calibration of the grism 1st and higher orders. Two WR stars were eventually selected from van der Hucht's (2001) catalogue, WR45 and WR96, whose magnitude ($14.8 < V < 14.14$) is bright enough to keep the exposure times shorter than 1 min. WR45 was observed during SMOV together with the HST standard star GD153 , while WR96 and the White Dwarf G191B2B were acquired during the INTERIM programme. GD153 and G191B2B were planned for achieving the flux calibration of the WFC G800L grism. As part of the ground tests, He+Ne arc lamps were observed in different positions on the WFC CCDs, namely the centre and near the amplifiers of chip 2 and chip1 to measure the field dependence of the grism dispersion and zero point. WR45 and GD153 were therefore observed at these same positions to verify the results obtained from the ground, and WR96 and G191B2B were imaged at the 'ground' positions plus five additional pointings, which we selected to ensure a good spatial coverage of the WFC field of view. Hereafter, we will focus on the grism wavelength calibration of the Wide Field Channel. The flux calibration of the WFC grims will be presented in Pirzkal et al. (2003, in preparation).

The observational strategy

Figure 1 shows the pointings in the WFC field of view used to monitor the field dependence of the grism dispersion correction and throughput (Prog. No. 9029, 9568 , PI Pasquali).

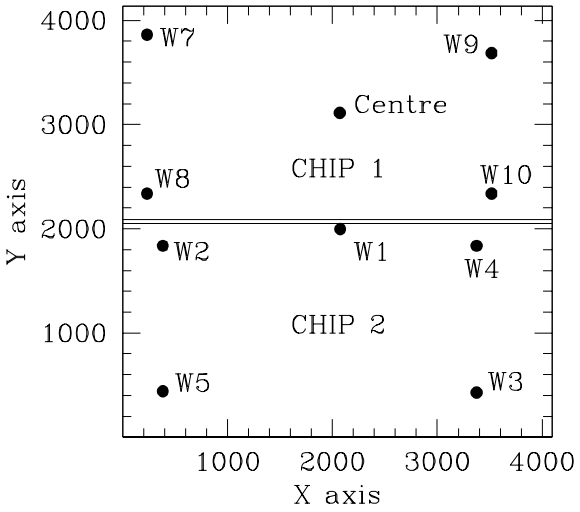

Figure 1: Map of the pointings used for WR45 and WR96 on the WFC aperture. Chip 1 is on top, chip 2 at the bottom.

The offset along the image X and Y axes of each pointing (in columns 2 and 3 of Table 1 within the full WFC aperture) with respect to the centre of a specific chip is described by a pair of POSTARG values. These were computed using the recipes in Mutchler & Cox (2001) and are listed in Table 1 in units of arcsecs.

POINTING	X POSITION (pixels)	Y POSITION (pixels)	POSTARG in X (arcsecs)	POSTARG in Y (arcsecs)
CHIP 1				
Centre	2072	3112	+0.0	+0.0
W7	234	3864	-91.16	+30.39
W8	234	2337	-91.16	-45.50
W9	3517	3687	+71.67	+34.07
W10	3517	2337	+71.67	-33.03
CHIP 2				
W1	2075	1998	+0.15	+48.42
W2	385	1837	-83.67	+34.00
W3	3376	429	+64.68	-24.62
W4	3376	1837	+64.68	+45.36
W5	385	440	-83.67	-35.43

Table 1. The POSTARG values adopted to position the spectra in the WFC field of view.

For each position, a pair of direct and grism images was acquired with the direct image taken through the F775W filter and in some cases the observation was repeated in the F625W filter to check the image position stability against the selected filters. Exposure times are listed in Table 2 for each target and spectral element. Repeated observations were executed at each position, either within the same visit or in different visits with the purpose of checking the repeatability of the filter wheel positioning.

TARGET	RA (J2000)	DEC (J2000)	F625W	F775W	G800L
WR45	11:38:05.2	-62:16:01.0	1 s	1 s	20 s
WR96	17:36:24.2	-32:54:29.0		1 s	20 s

Table 2. The J2000 coordinates of the SMOV targets and the exposure times adopted for each star and spectral element of the WFC.

The images were read as subarrays (3000 pixels in X and 400 pixels in Y) in order to reduce the read-out overhead of the chips. The SMOV and INTERIM datasets are listed in Appendix A.
Mono dimensional spectra were extracted using the ST-ECF aXe code (Pirzkal et al. 2001) where the width of the extraction aperture was set to 2 pixels and the background was taken at a distance of +/- 60 pixels from the spectral trace.

The physical properties of the grism

A number of grism properties can be measured directly in the raw images: the tilt of the spectrum, the length of the grism orders and their separation from the 0^{th} order, the (X,Y) -shifts between the 0^{th} order and the target position in the direct image. In addition, the available set of pointings allows to determine the field dependence of the above parameters across the WFC chips, and hence to quantify the geometric distortions affecting the grism data. While the (X,Y)-shifts and the tilt are the requisites for finding and tracing spectra, the length and separation of the orders are used to define the size of the extraction aperture along the dispersion axis.

1. The spectral tilt

We have measured the (X,Y) coordinates of the emission line peaks along the whole spectrum of WR45 and WR96 (from the -3^{rd} to the $+3^{rd}$ order) and fitted the pairs with a first-order polynomial, to determine the slope of the spectrum with respect to the X axis. The X axis is in fact close to the direction of the dispersion axis. We have averaged the tilts computed for each observed position on the chips and obtained standard deviations smaller than $\sigma = 0^{o}.02$.

The spectrum tilt at the center of the f.o.v, W1, is $-1^{o}.911$; the average value over the whole field of view of the WFC is $-1^{o}.983 +/- 0^{o}.337$. An increase of $1^{o}.09$ in the spectrum tilt is observed along the diagonal from W7 to W3, equivalent to 57% of the value measured at the central position W1. Similarly, from W9 to W5 the tilt increases by $0^{o}.79$, about 41% of the value measured in W1. The amplitude and direction of the tilt variations are likely due to the geometric distortions of the ACS. Indeed, the projected pixel linear size and area in direct images increase along the diagonal from W7 to W3 by ~ 9% each. The field dependence of the tilt is sketched in Figure 2.

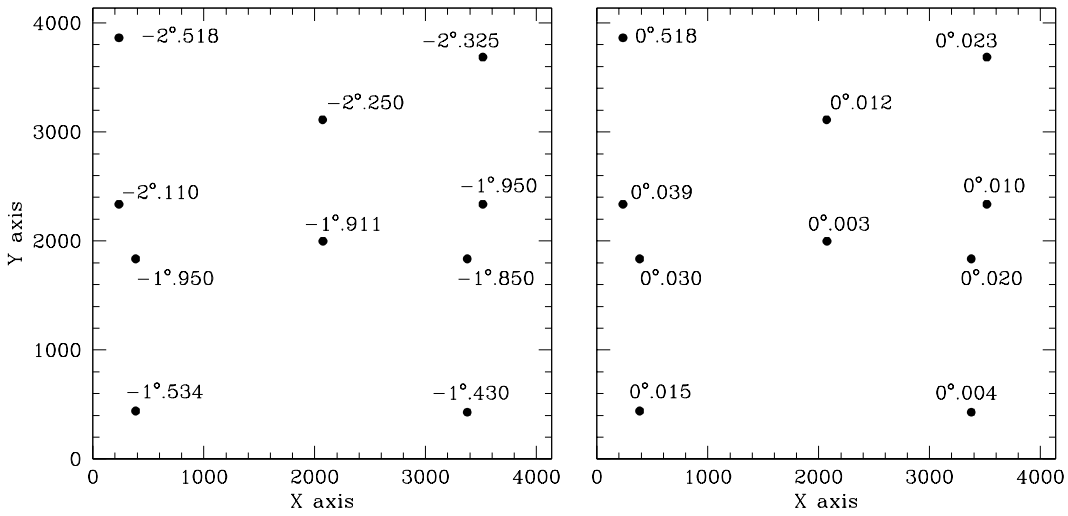

Figure 2: The spectrum tilt (left) and its standard deviation (right) are plotted as a function of pointing across the WFC field of view. Both chips are shown back-to-back.

2. The length of the grism orders

In order to measure the length in pixels of each grism order, a threshold has to be set in the counts which distinguish the target emission from the background. We have estimated the background in areas in the grism image free of spectra and fixed the threshold at a 3σ level above the background. Pixels whose counts are larger than this threshold are assigned to the target spectrum. The measurements have also been performed on the continuum spectra of the standard stars.

The grism 0^{th} order (which falls outside the image edges in W7) is dispersed over 23 pixels on average, with a standard deviation of 0.8 pixels across the field of view which rules out any significant field dependence. This is true also for the 0^{th} order FWHM, whose mean value is 4.4 +/ 0.3 pixels. The nominal spectral range from 0.5 to 1 μm determines for the 0^{th} order a spectral dispersion of ~ 260 A/pix. Therefore, the emission line spectra obtained in SMOV and INTERIM are not suitable to measure the in-orbit dispersion of the the 0^{th} order. The length of the first and second grism orders is listed in Table 3 in pixel units; the values are an average among the pointings. The 2^{nd} order should be about two times longer than the 1^{st} order, but the very low sensitivity of the grism at longer wavelengths prevents the detection of this order at $\lambda > 8000$ A.

	1st Ord.	**2nd Ord.**	**-1st Ord.**	**-2nd Ord.**
LENGTH	156	125	102	111

Table 3. The length (in pixels) of the grism first and second orders as averaged over the whole field of view.

The separation of the grism first and second orders from the 0^{th} (peak wavelength at ~ 6000 A) is reported in Table 4. The order separation is measured along the image X axis, and indicates the distance between the light centroid of the 0^{th} order and the first pixel of the n^{th} order which turns to be 3σ above the background.

	1^{st} Ord.	**2^{nd} Ord.**	**-1^{st} Ord.**	**-2^{nd} Ord.**
SEPARATION from 0^{th} order	93	251	-122	-247

Table 4. The separation in pixels of the grism first and second orders from the 0^{th}.

3. The (X,Y)-shifts

They are defined as the difference in the (X,Y) coordinates between the object position in the direct image and the position of the 0^{th} order in the grism image. Since the spectra are

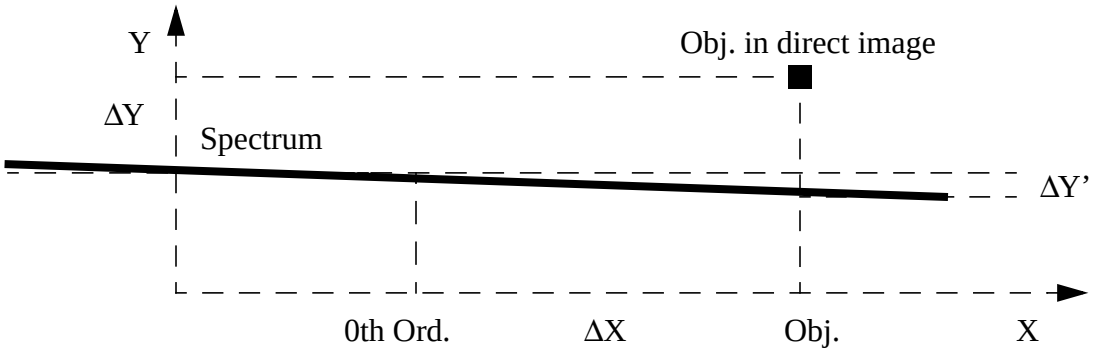

Figure 3: a schematic plot of the geometry involved in finding and tracing spectra in the grism image.

tilted, the (X,Y) shifts between the 0^{th} order and the object in the direct image are not sufficient to locate the spectrum in the grism image. An extra term, $\Delta Y' = \Delta X * TANG(TILT)$, is needed so that the spectrum is found at: $\Delta Y + \Delta Y'$ from the object position in the direct image, as shown in Figure 3.

Except for the W7 and W8 positions whose 0^{th} order falls outside the physical boundaries of the image, the (X,Y) shifts have been measured for all the pointings across the f.o.v. The average values, obtained from the observations repeated at each position on the chip, are plotted in Figure 4. It appears that the Y-shift increases along the W5 - W9 diagonal by a factor of two, which would indicate that the increase is real and not an artifact of the measurements procedure.

When using these quantities, one has to make sure that the telescope pointing and the filter wheel positioning are accurate enough to consider the measured shifts stable in time. From the observations repeated at each pointing, it turns out that the repeatability of the

object position in the direct image and the position of the 0th order in the grism image occurs within 2 pixels. If we consider the grism 1st order at a spectral resolution of ~ 39 A/pix, an uncertainty of 2 pixels does not significantly compromise the spectral dispersion, but it affects the zero point of the wavelength solution, by introducing a shift of about 78 A. This would correspond to a 0.01 error on the object redshift as computed from the 1st order spectrum at λ = 7500 A.
The SMOV and INTERIM data also show that the repeatability of the object position in the direct image does not depend on the filter selected for imaging.

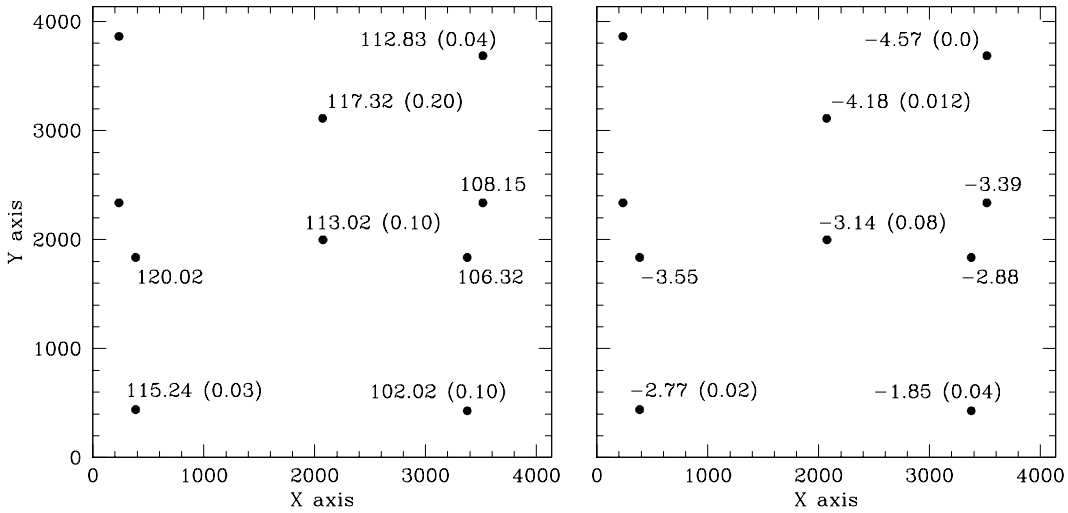

Figure 4: The shift in the X (right) and Y (left) coordinates between the object position in the direct image and the position of the 0th order in the grism image across the f.o.v. The units are pixels. These values are averages among repeated observations and the relative standard deviations are in brackets.

The wavelength calibration: the method

Wavelength solutions were derived for the W1, W3, W5, W7, W9 positions during the ground tests which made use of arc lamps. We have applied them to the extracted spectra of WR45 and WR96 in order to measure their mean line FWHM in Angstroms. In the raw spectra, the mean line FWHM turns out to be 2.9, 4.2 and 5.9 pixels in the grism 1^{st,} 2nd and 3rd orders; 2.6, 3.7 and 6.4 pixels in the grism negative 1st, 2nd and 3rd orders. For the sake of comparison, in the spectra calibrated with the arc lamp wavelength solutions, the mean line FWHM is 120.1 A, 92.8 A, 86.4 A in the 1st, 2nd and 3rd orders. These values, however, do not represent the instrument line PSF alone, since they have been measured from lines broadened by stellar winds, and these winds are partially resolved by the WFC/grism (cf. Pasquali et al. 2001). Moreover, the observed lines are severely blended at least in the grism +/-1st orders, and this introduces an additional source of uncertainty in the measurement of the line FWHM.

We have convolved the high resolution spectra of WR45 and WR96 obtained from the ground (cf. Pasquali et al. 2001) with these average FWHMs, reidentified the blends in the "degraded-resolution" template and measured their wavelength after "degradation". A wavelength table has then been produced for cross-identification with the ACS spectra of WR45 and WR96, and fitted against the line peaks in pixels in the extracted spectra. The fitting routine (POLYFIT in IRAF) relies on a sample of 7 lines for the 1st, 3rd and -1st orders, 3 to 5 lines for the 2nd, -2nd and -3rd orders. Therefore, we have fitted wavelengths vs. pixels with a first order polynomial for all the orders except the 1st one, for which we have used a second order polynomial. Although at lower resolution, the 1st orders are characterized by a very high S/N ratio which allows to represent their wavelength solutions with a second order polynomial. Such a polynomial reduces the RMS of the fit by a factor of 2 with respect to the first order polynomial and fits better the blue and red edges of the 1st order spectrum. This procedure was applied to each spectrum for each pointing and for each order between -3rd and +3rd, and the final results, such as dispersion and zero point, were averaged for each order and each position in the f.o.v. These mean parameters define the wavelength solutions that are used by the ST-ECF extraction package aXe.

The wavelength calibration: the results

The grism 1st order

Figure 5 shows the grism 1st order spectrum of WR45 as simulated with SLIM 1.0 (left panel, cf. Pasquali et al. 2001) and observed with the WFC (right panel). The spectra look

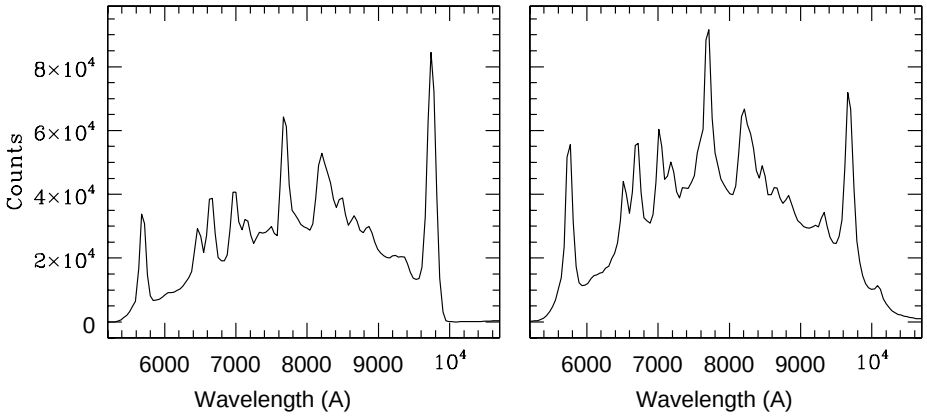

Figure 5: the 1st order spectrum of WR45 as simulated with SLIM 1.0 (10 s, left panel) and observed with the WFC (20 s, right panel). The background has been subtracted.

almost identical, exception made for the grism response which appears to be more sensitive in the blue than predicted. The grism 1st order spectra of WR45 (left) and WR96 (right) are shown in Figure 6.

The wavelength solutions determined for the grism 1st order are plotted in Figure 7 as a function of position on the chip. Each one is expressed as a second order polynomial of the form: $\lambda = \Delta\lambda_0 X + \Delta\lambda_1 X^2 + \lambda_0$, where X is the difference between the position along the spectral trace and the position of the object in the direct image. In Figure 7, the individual $\Delta\lambda_0$, $\Delta\lambda_1$ and λ_0 values are an average among the spectra observed in the same position (on the left), and their corresponding standard deviations are plotted on the right. The standard deviations have been computed by propagating the errors arising from the fits of a second order polynomial to the tables of the cross-identified wavelengths and pixels. The $\Delta\lambda_0$, $\Delta\lambda_1$ and λ_0 values averaged across the field of view are in Table 5 together with their scatter and the typical RMS of the fits. The mean dispersion of the grism $\Delta\lambda_0$ is 39.18 A/pix with a standard deviation of about 3 A/pix. This implies that the variation in the local dispersion seen across the field of view is real and likely due to the geometric distortions of the ACS. The field dependence of the dispersion develops along the diagonal from the W7 to the W3 position and has an amplitude of about 22% of the dispersion measured in W1. In other words, the dispersion varies by 11% from the centre to the edges of the field of view leaving the right bottom corner with the lowest dispersion across the WFC. A 14% decrease of $\Delta\lambda_0$ can also be recognized between W5 and W1.

Since the FWHM of the lines in the WFC/grism spectra is not purely instrumental, but convolved with the stellar winds of WR45 and WR96, a resolving power *R* defined as (λ/FWHM) could be somewhat misleading. Therefore, we have adopted $R = (\lambda/2\Delta\lambda)$ which has to be considered not only an upper limit to the grism resolving power, but also more a measure of the grism sampling rather than its resolution.

PARAMETERS	MEAN	StD of the mean
$\Delta\lambda_0$ (A/pix)	39.18	2.69
$\Delta\lambda_1$ (A/pix^2)	0.010	1.56e-03
λ_0 (A)	4790.26	18.14
RMS of the fit (A)	3	

Table 5. The wavelength solution for the grism 1st order averaged across the field of view together with its standard deviation. The RMS of the fitting procedure is also reported.

A mean dispersion of 39.18 A/pix corresponds to $R = 96$ at $\lambda = 7500$ A. Across the WFC field of view, *R* decreases from ~107 in W7 to ~85 in W3. In the case of the mean, second-term dispersion, $\Delta\lambda_1$, its standard deviation in Table 5 is comparable with the fitting uncertainty at each position, so that no field dependence can be really claimed. Only the $\Delta\lambda_1$ value measured in W7 differs from the others, being smaller by about 30%. No specific monothonic trend can be identified across the f.o.v. for the zero point λ_0.

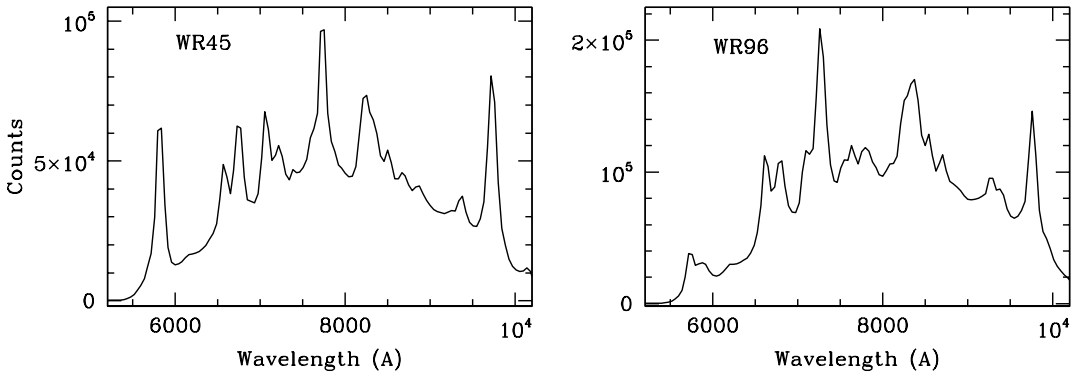

Figure 6: The grism 1st order spectra of WR45 (left) and WR96 (right).

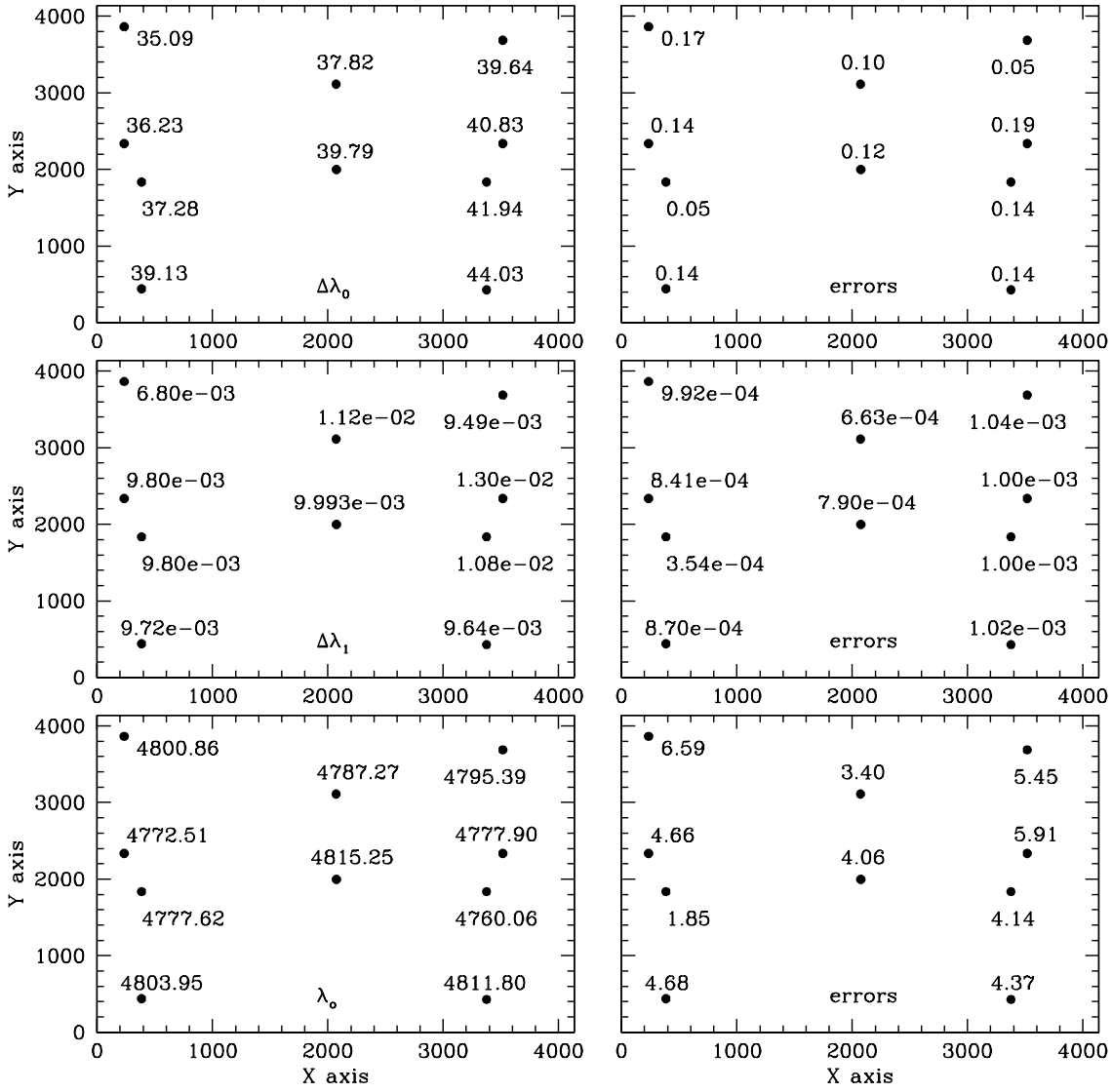

Figure 7: The wavelength solutions calculated for the G800L grism 1st order at different positions in the field of view of the WFC.

The grism 2nd order

The 2nd order spectrum of WR45 and WR96 acquired in the W1 position is shown in Figure 8. The spectrum overlaps with the 1st order at about λ = 5400 A and its sensitivity response becomes very low redward of 8000 A. For this reason we derived the wavelength solution of the 2nd order in the spectral range between 5500 A and 8000 A.
The wavelength solution has been fitted with a first order polynomial $\lambda = \Delta\lambda_0 X + \lambda_0$.
The dispersion corrections computed for the different pointings are summarized in Figure 9.

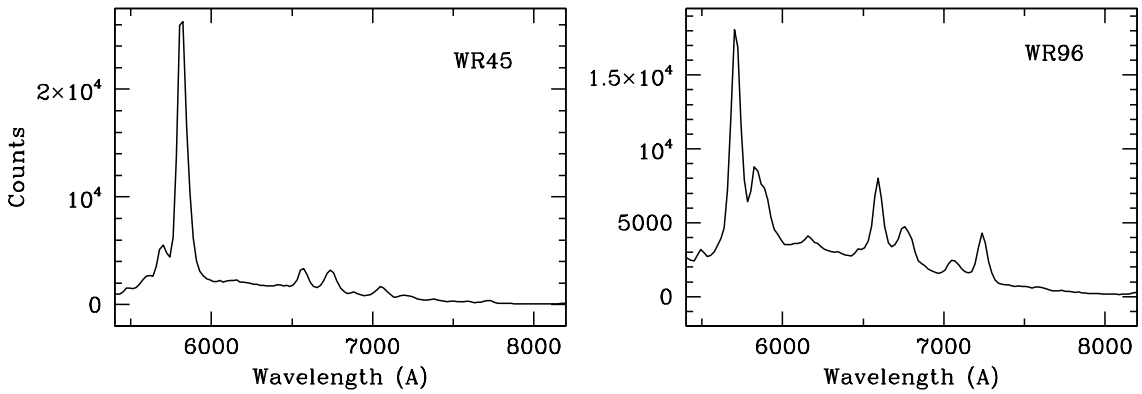

Figure 8: The grism 2nd order spectra of WR45 (left) and WR96 (right), obtained in position W1 and with an exposure time of 20 s. The background has been subtracted.

The dispersion and the zero point as averaged across the f.o.v are to be found in Table 6 with the RMS of their fits and the standard deviation on the mean $\Delta\lambda_0$ and λ_0.

On average, the grism 2nd order is characterized by a dispersion of 20.54 A/pix corresponding to R ~ 158 at λ = 6500 A. The standard deviation associated with this value is 1.3 A/pix . As for the 1st order, the dispersion is seen decreasing from the W7 to the W9 position, by a factor of about 22% of the value measured in W1, or 11% from the centre to the corner positions above. Similarly, the resolving power decreases from ~ 355 to ~ 284 at λ = 6500 A. A minor decrease of 1% in $\Delta\lambda_0$ can be seen in the W5-to-W1 direction. The only trend visible in λ_0 is the increase along the W7-W3 diagonal, by a factor 1.4% of the value measured in W1, which is also four times the mean RMS of the fit.

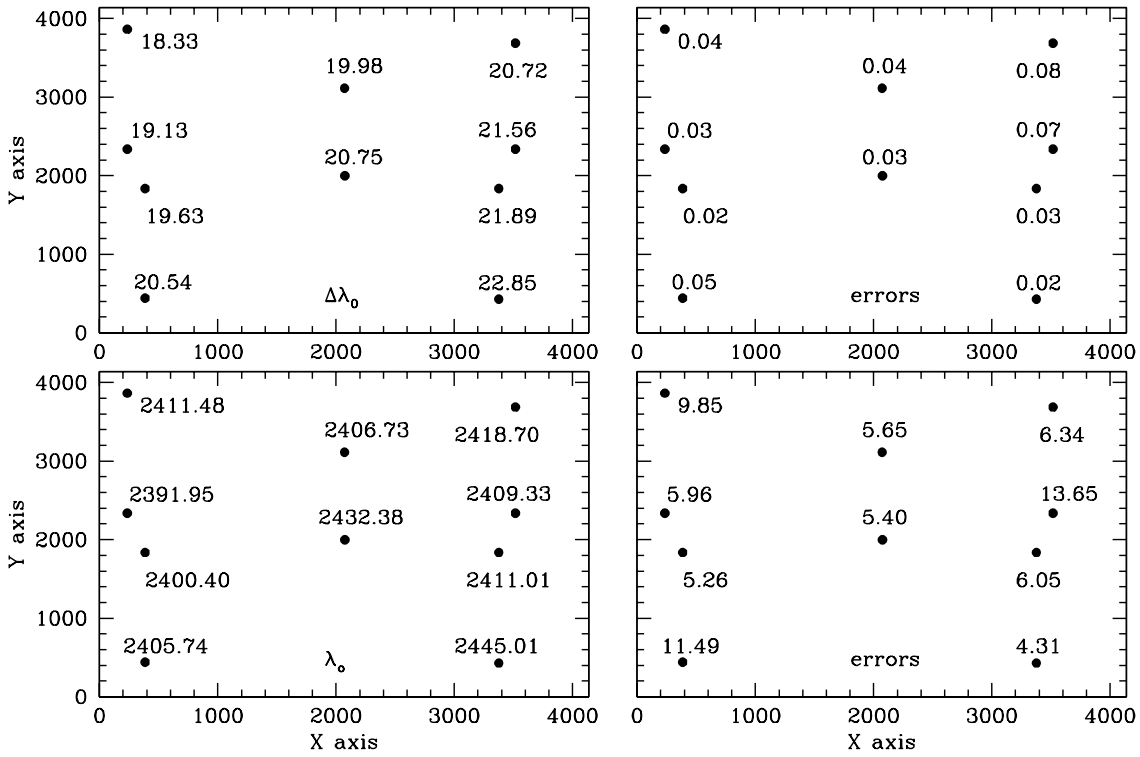

Figure 9: The wavelength solution of the grism 2nd order as a function of pointing. Left panel: the dispersions $\Delta\lambda_0$ and zero points λ_0, right panel: standard deviations.

	MEAN	**StD of the mean**
$\Delta\lambda_0$ (A/pix)	20.54	1.34
λ_0 (A)	2413.27	15.44
RMS of the fit (A)	3	

Table 6. The mean dispersion and zero point of the grism 2nd order across the f.o.v.

The grism 3rd order

An example of the grism 3rd order spectrum obtained for WR45 and WR96 in position W7 is plotted in Figure 10, while the spatial map of its dispersion and zero point is in Figure 11.

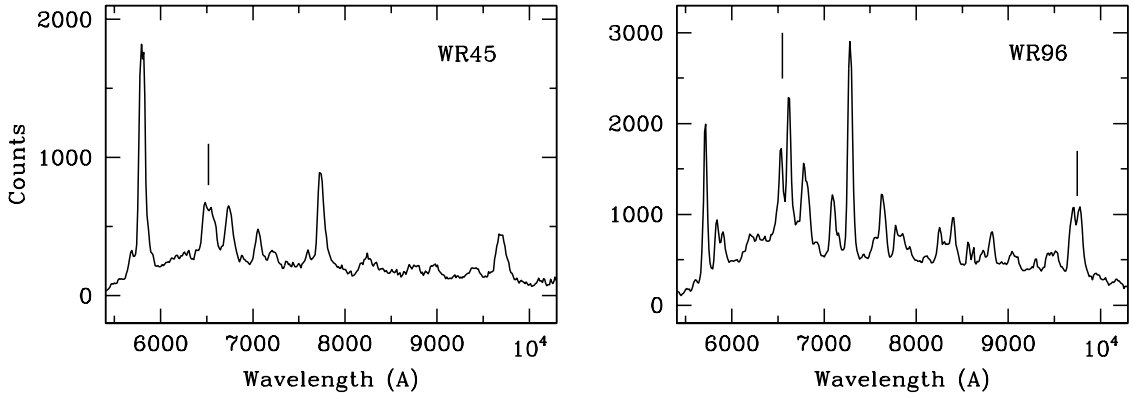

Figure 10: The grism third order spectrum obtained for WR45 and WR96 in the W7 position for an exposure time of 20 s. The background has been subtracted.

A number of lines are identified in Figure 10 which appear to be split when compared to the high resolution spectra taken from the ground. The line splitting is most likely due to the de-focussing of the higher grism orders.

The dispersion correction of the 3rd order has been derived in the form of a first order polynomial: $\lambda = \Delta\lambda_0 X + \lambda_0$. The values in Table 7 are averaged among all the observations available for each position; their standard deviations take also into account the fit uncertainties via error propagation.

POSITION	$\Delta\lambda_0$ (A/pix)	ERROR on $\Delta\lambda_0$	λ_0 (A)	ERROR on λ_0
W1	14.33	0.03	1496.02	13.23
Centre	13.60	0.02	1554.07	5.97
W2	13.38	0.02	1546.68	10.11
W3	15.76	0.04	1513.70	12.43
W4	14.88	0.02	1564.48	6.88
W5	14.16	0.05	1479.14	19.42
W7	12.65	0.05	1483.25	18.11
W8	13.06	0.02	1531.34	7.51
W9	14.23	0.04	1506.60	18.00
W10	14.62	0.02	1569.80	7.09

Table 7. The wavelength solution of the 3rd order as a function of position across the WFC f.o.v.

The mean values (overall the WFC aperture) of $\Delta\lambda_0$ and λ_0 from Table 7 are listed in Table 8 with their standard deviation and the typical RMS of our fitting procedure.

	MEAN	**StD of the mean**
$\Delta\lambda_0$ (A/pix)	14.07	0.92
λ_0 (A)	1524.51	33.45
RMS of the fit (A)	12	

Table 8. The average dispersion and zero point of the grism 3rd order.

We have derived for the grism 3rd order an average dispersion of 14.07 A/pix equivalent to a resolving power $R \sim 249$ at $\lambda = 7000$ A. The usual trend of decreasing resolution is present here as well, from the W7 ($R \sim 277$) to the W3 ($R \sim 222$) position. The amplitude of such a variation in $\Delta\lambda_0$ is ~22% of the value measured in W1, or 11% from the centre to the chip corner. Along the other diagonal, from W5 to W1, a slight decrease of $\Delta\lambda_0$ of about 1.2% is detected. The zero point λ_0 increases by 2% of the value derived for W1 going from W7 to W3; it corresponds to two times the standard deviation on the mean λ_0 in Table 7.

The grism -1st order

The grism -1st order detected in the central position W1 is shown in Figure 11 for WR45 and WR96. The -1st order of the grism is present in all the positions on the chips, except W7 where its location falls outside the physical boundaries of the image. The spatial map of its dispersion correction is plotted in Figure 12, and its mean dispersion correction is summarized in Table 9. The wavelength solution is again of the form: $\lambda = \Delta\lambda_0 X + \lambda_0$. The spectral resolution in the -1st order is lower than in the 1st one, and the corresponding

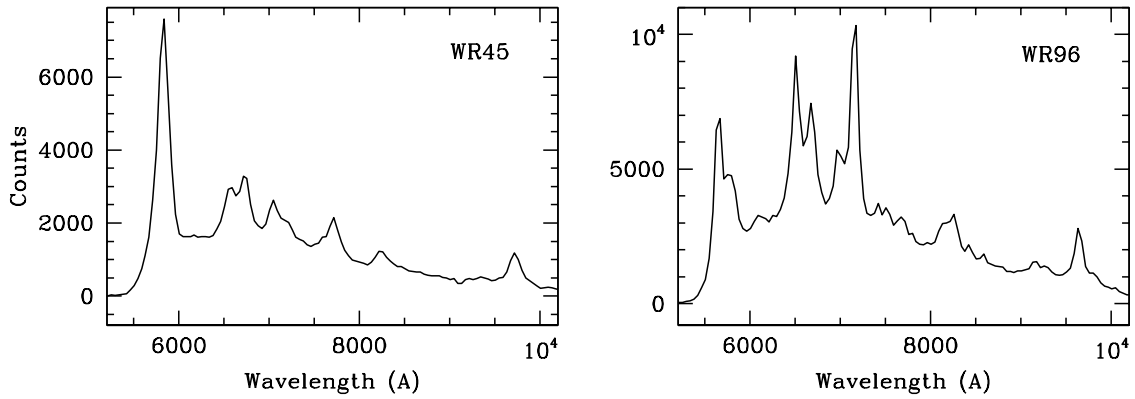

Figure 11: The grism -1st order spectra of WR45 (left) and WR96 (right) in the W1 position, obtained with an exposure time of 20 s. The background is subtracted.

resolving power is ~ 87. Missing the measurements in W7, we can only notice a change in the dispersion between W1 and W3, of the order of 11% the value in W1. The same can be said for the zero point which decreases by 1% from W1 to W3. No clear, monothonic trend is seen between the W5 and W9 positions.

	MEAN	**StD of the mean**
$\Delta\lambda_0$ (A/pix)	-42.51	2.22
λ_0 (A)	-4879.92	87.11
RMS of the fit (A)	9	

Table 9. The mean wavelength solution for the -1st order across the field of view of the WFC.

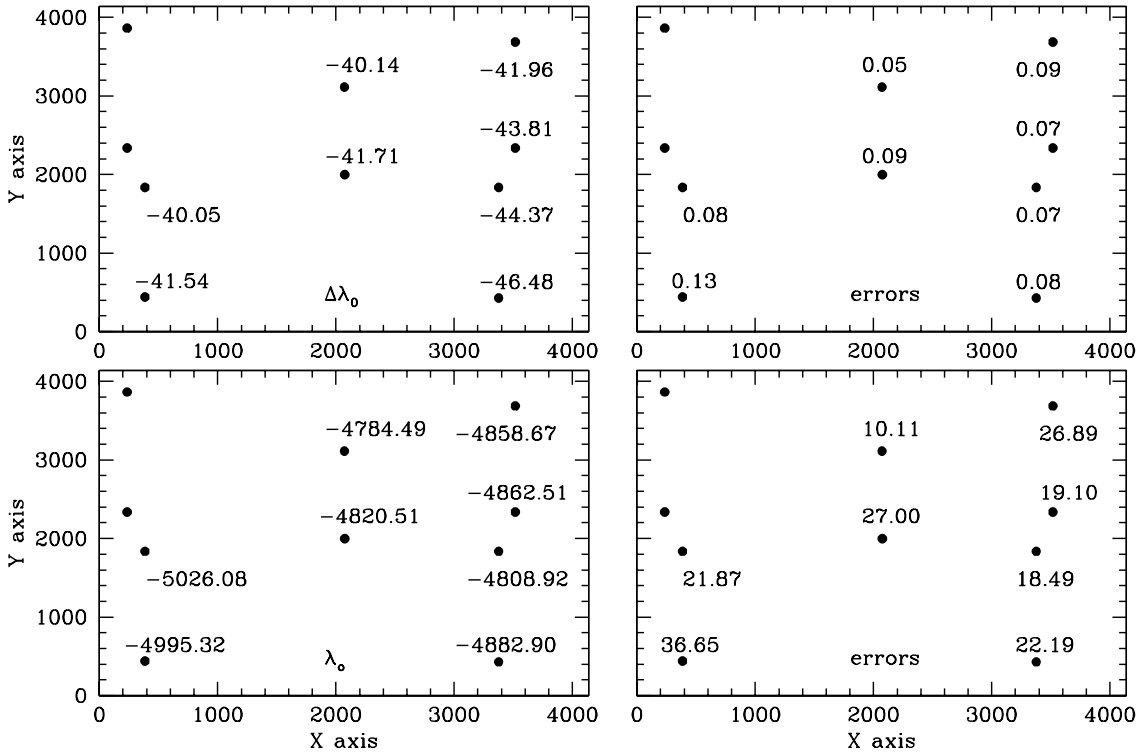

Figure 12: The spatial map of the -1st order dispersion and zero point (left column). These values are averaged among the observation taken for each position and their corresponding standard deviations are plotted in the right column.

The grism -2nd and -3rd orders

An example of the grism -2nd and -3rd orders is shown in Figure 13 for WR45 and WR96, and their dispersion correction (in the form of a first order polynomial) is listed in Table 10 as a function of position on the WFC chips. A mean (overall the WFC f.o.v) wavelength solution has been derived for both orders, and the mean dispersion and zero point are reported in Table 11.

The resolving power of the -2nd and -3rd orders is R = 153 at λ = 6500 A and 254 at λ = 7000 A, respectively. A 11% variation is detected in the dispersion from the W1 to the W3 position and for both orders. It is indeed significant, since the error on the dispersion from the fitting procedure in W1 and W3 is about 0.1 A/pix. The zero point of the wavelength solution of the -2nd order does not show any field dependence as the standard deviation on the mean zero point is within the errors. On the contrary, the zero point of the -3rd order decreases by 3% from W1 to W3 and the variation (about 43 A) is at a 4σ level, where σ is assumed to be 11.5 A from the W1 position.

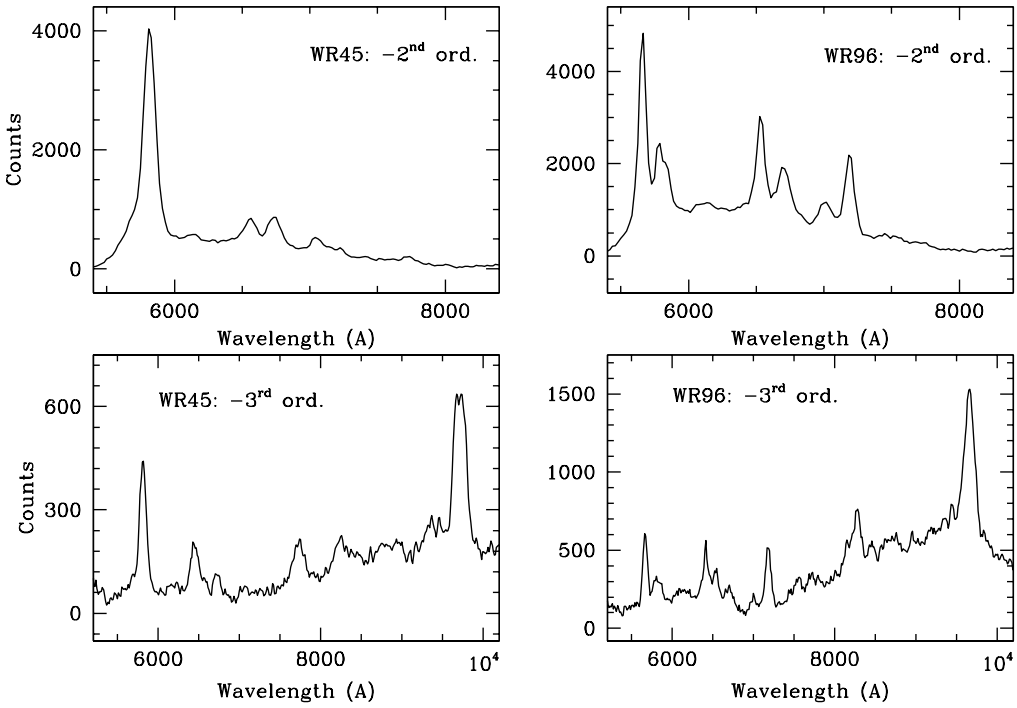

Figure 13: The WR45 and WR96 grism -2nd (top) and -3rd (bottom) order spectra.

Table 10: the wavelength solutions for the -2nd and -3rd orders as a function of position across the WFC f.o.v.

POSITION	$\Delta\lambda_0$ (A/pix)	ERROR on $\Delta\lambda_0$	λ_0 (A)	ERROR on λ_0
-2nd Order				
W1	-20.50	0.08	-2340.04	36.90
Centre	-19.86	0.08	-2385.66	24.52
W2				
W3	-22.77	0.06	-2351.32	23.51
W4	-21.96	0.09	-2400.35	37.85
W5				
W7				
W8				
W9	-20.62	0.05	-2365.09	21.48
W10	-21.60	0.07	-2402.27	29.80
-3rd Order				
W1	-13.25	0.11	-1370.24	11.51

POSITION	$\Delta\lambda_0$ (A/pix)	ERROR on $\Delta\lambda_0$	λ_0 (A)	ERROR on λ_0
Centre	-12.90	0.02	-1456.94	9.48
W2				
W3	-14.80	0.01	-1413.63	3.90
W4	-14.20	0.004	-1423.91	2.73
W5				
W7				
W8				
W9	-13.37	0.01	-1407.96	5.64
W10	-13.97	0.06	-1434.05	35.70

Table 10: continued.

-2nd Order	MEAN	StD of the mean
$\Delta\lambda_0$ (A/pix)	-21.21	1.08
λ_0 (A)	-2374.12	26.00
RMS of the fit (A)	5	
-3rd Order		
$\Delta\lambda_0$ (A/pix)	-13.75	0.70
λ_0 (A)	-1417.79	29.01
RMS of the fit (A)	3	

Table 11. The mean dispersion and zero point of the wavelength solution for the grism -2nd and -3rd order. The average has been performed on the ten positions available on the chips.

The calibration files for aXE

The measurements described in this document were used to create configuration files for the ST-ECF slitless spectroscopy extraction software aXe (Pirzkal et al. 2001). aXe is able to account for the field dependence of extraction parameters as long as that field dependence can be adequately modeled using an n^{th} order 2D polynomial.

We have separately fitted the tilt, (X,Y)-shifts, wavelength zero points, and the first and second order wavelength dispersion coefficients as a function of the (X,Y) position of the

target in the direct image and to second order 2D polynomials. As these extraction parameters vary smoothly as a function of position in the detector, a set of 2D polynomials was able to properly fit the SMOV and INTERIM data. The residual to the fit are quite small: Table 12 shows the residuals to the fit for the first order dispersion.

PARAMETER	ERROR
ΔX	0.15 pix
ΔY	0.10 pix
TILT	$0^o.03$
λ_0	15.78 A
$\Delta\lambda_0$	0.6%
$\Delta\lambda_1$	2.20%

Table 12. The residuals to the 2D fit for the field dependence of the 1st order dispersion correction.

The 2D fits for the field dependence of the grism 1st order λ_0, $\Delta\lambda_0$ and $\Delta\lambda_1$ are plotted in Figure 14, as an example.

A set of aXe WFC configuration files (one for each chip) containing field dependent descriptions of the positive and negative spectral orders of the WFC grism mode have been created and can be obtained from the aXe web pages at http://www.stecf.org/software/aXe/.

In order to prove the consistency of the procedure adopted for determining the grism wavelength calibration and its field dependence, we have mosaiced the single grism subarrays (not drizzled and not corrected for geometric distortions) obtained during INTERIM into a full 2048 x 4096 frame for each chip, and re-extracted with aXe the wavelength calibrated spectrum of WR96 at each pointing (cf. Figure 1). The wavelength calibration was performed using the surface fits of Figure 14. The spectra obtained at the Centre and in W7, W8, W9 and W10 (Chip 1) are plotted in Figure 15, while those observed in W2, W3, W4 and W5 (Chip 2) are in Figure 16. The spectra have been scaled vertically, as their flux unit is counts/pixel and not count/Angstrom. The overlap of the spectra occurs in less than 0.5 pixels.

Conclusions

Simulations based on high resolution spectra taken from the ground showed that Wolf-Rayet stars of WC subtype provide a reasonably good wavelength calibration of the ACS grism when coupled with the WFC. The calibration targets were selected to be WR45 and WR96, observed during the SMOV and INTERIM tests, respectively. The observational

strategy was designed to perform multiple observations of the same target across the field of view of the WFC and thus provides the spatial mapping of the grism physical properties and grism wavelength solution. It is indeed well known that ACS/WFC suffers severe geometric distortions, which affect not only the pixel size but also the illumination pattern of the chips such that the pixel scale increases along the diagonal from the top left corner to the bottom right corner by ~9% (Cox & Lindler 2002).

The data sets were analyzed with IRAF and spectra were extracted with the ST-ECF extraction package aXe. The results, obtained for non-drizzled spectra which have not been corrected for geometric distortions, can be summarized as follow:

- The grism 0^{th} order is displaced from the target in the direct image by <-111.87> +/- 6.00 pixels along the X axis, and <+3.29> +/- 0.85 pixels in the Y direction. While the X offset

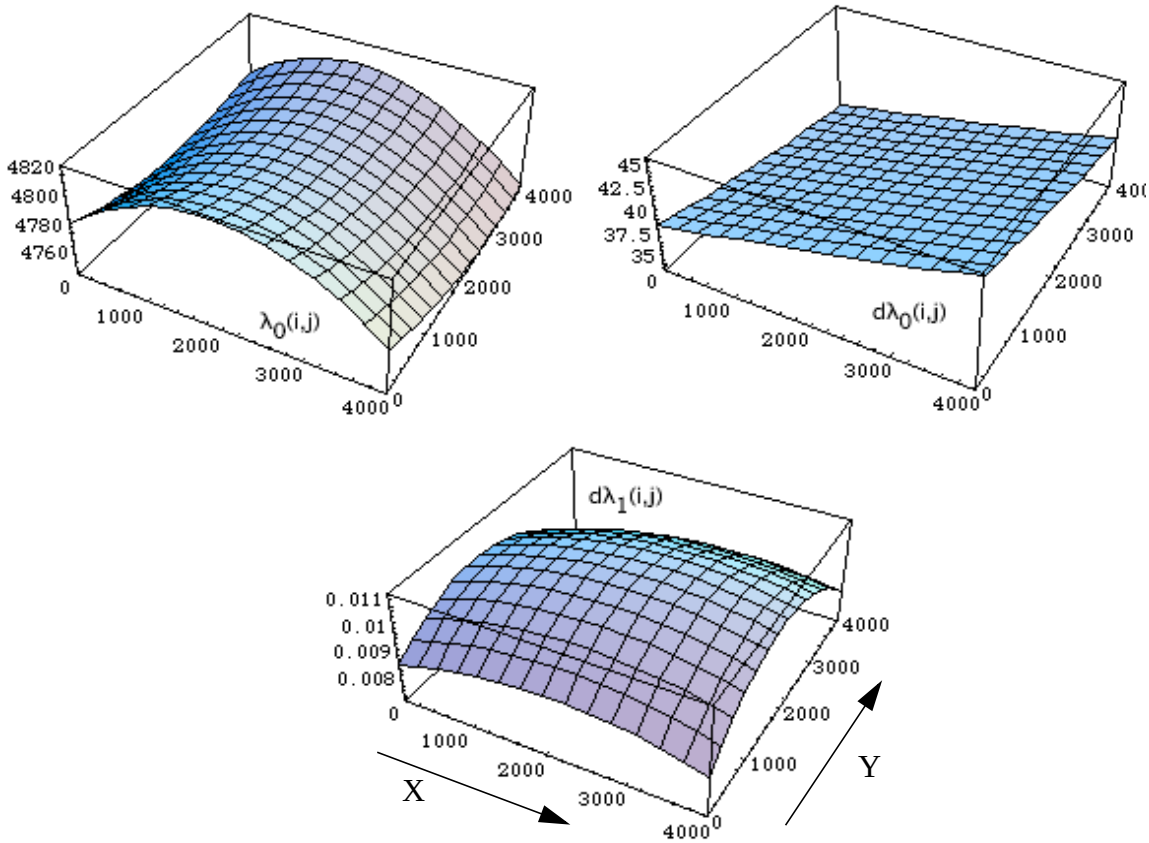

Figure 14. The 2D fits for the field dependence of the grism 1^{st} order. Plotted are the first and the second terms of the dispersion ($\Delta\lambda_0$ and $\Delta\lambda_1$) and the wavelength zero point (λ_0).

seems independent of the position in the f.o.v, the shift in the Y direction increases (in absolute value) for increasing Y coordinate.

- The spectrum tilt is on average -1^{o}.983 +/- 0^{o}.337 and is field-dependent. It varies by 1^{o}.09 from the left top corner to the right bottom corner of the WFC f.o.v, and by 0^{o}.79 from the left bottom corner to the right top corner.
- The 0th order is characterized by a mean FWHM of 4.4 pixels and a mean length of 23 pixels along the image X axis, with no significant field dependence. The 0th order FWHM along the image Y axis is ~ 2 pixels, comparable with the WFC PSF. The length and the separation (from the 0th order) of the grism higher orders are reported in Tables 2 and 3.
- At a distance of about 360 pixels (18 arcsec) from the 0th order, the 3rd order appears de-focussed. The out-of-focus produces split lines whose peaks are resolved at a dispersion of ~14.2 A/pix.
- The wavelength solution of the grism 1st order is fitted with a second order polynomial and a RMS of about 3 A. The dispersion solution of the positive higher orders and the negative ones is fitted with a first order polynomial with an RMS varying between 3 A (2nd order) and 12 A (3rd order). The final wavelength solutions, as obtained at the centre of the WFC aperture (W1), are summarized in Table 13.
- The coefficients of the dispersion corrections derived across the WFC field of view for each order, the (X,Y)-shifts of the 0th order from the target in the direct image and the spectrum tilt are fitted with second order 2D polynomials and as a function of the (X,Y) position of the target in the direct image. These 2D polynomials, which represent the field dependence of the grism wavelength solution, are stored in appropriate calibration files, used by the ST-ECF extraction package aXe.

GRISM ORDER	**FIRST TERM DISPERSION (A/pix)**	**SECOND TERM DISPERSION (A/pix^2)**	**ZERO POINT (A)**
First	39.79	0.00993	4815.25
Second	20.75		2432.38
Third	14.33		1496.02
Negative First	-41.71		-4820.51
Negative Second	-20.50		-2340.04
Negative Third	-13.25		-1370.24

Table 13. The wavelength solutions obtained for position W1 (centre of the WFC aperture).

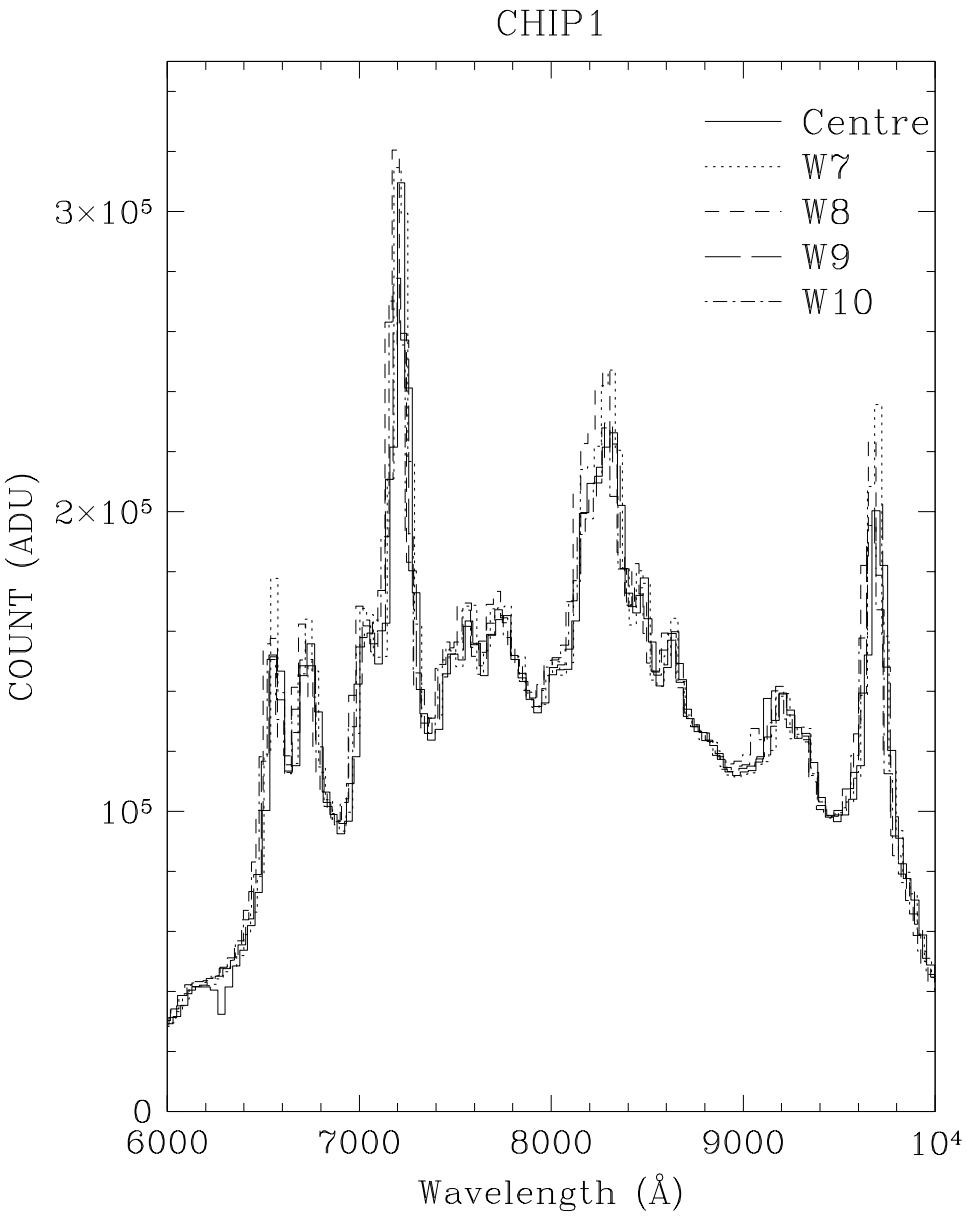

Figure 15. The spectra of WR96 obtained at the Centre and in W7, W8, W9 and W10 of Chip 1. The wavelength calibration was performed using the surface fits of Figure 14.

References

Cox, C., Lindler, D., 2002, ISR ACS 2002-02 “ACS Distortion derived from RAS-HOM Measurements”

van der Hucht, K.A., 2001, “The VIIth catalogue of galactic Wolf-Rayet stars”, New AR, 45, 135

Mutchler, M., Cox, C., 2001, STScI ISR ACS 2001-07 “ACS dither and mosaic pointing patterns”

Pasquali, A., Pirzkal, N., Walsh, J.R., 2001, ST-ECF ISR ACS 2001-04 “Selection of Wavelength Calibration Targets for the ACS Grism”
Pirzkal, N., Pasquali, A., 2001, ST-ECF Newsletter, 28, “SLIM - grism simulator for the ACS”, p. 3
Pirzkal, N., Pasquali, A., Demleitner, M., 2001, ST-ECF Newsletter, 29, “Extracting ACS Slitless Spectra with aXe”, p. 5

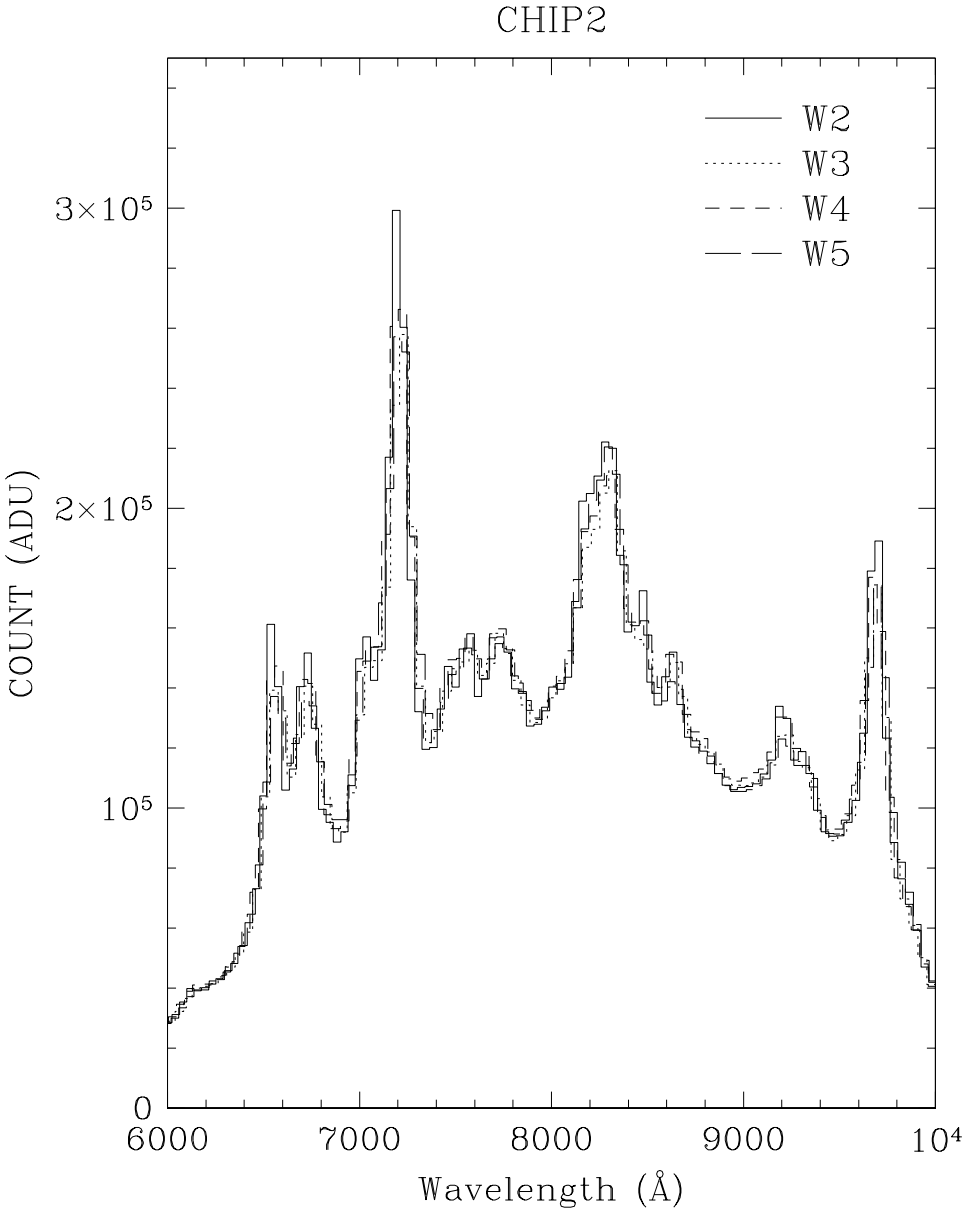

Figure 16. As in Figure 15 but for the WR96 spectra acquired in Chip 2.

Appendix A

The datasets acquired during SMOV (Prog. No. 9029, PI Pasquali) are listed in Table 14, while the direct and grism images taken during the early Cycle 11 INTERIM calibrations (Prog. No. 9568, PI Pasquali) are reported in Table 15.

Table 14. The SMOV observations

FITS FILE	TARGET	ELEMENT	POINTING
j8ca02pfq	WR45	F775W	W1
j8ca02pgq	WR45	G800L	W1
j8ca02phq	WR45	F775W	W1
j8ca02piq	WR45	G800L	W1
j8caa2pqq	WR45	F775W	W1
j8caa2prq	WR45	G800L	W1
j8caa4aoq	WR45	F625W	W1
j8caa4apq	WR45	G800L	W1
j8caa2plq	WR45	F775W	W3
j8caa2pmq	WR45	G800L	W3
j8caa2pnq	WR45	F775W	W3
j8caa2poq	WR45	G800L	W3
j8caa4alq	WR45	F625W	W3
j8caa4amq	WR45	G800L	W3
j8cab1a2zq	WR45	F775W	W3
j8cab1b0q	WR45	G800L	W3
j8ca02p9q	WR45	F775W	W5
j8ca02paq	WR45	G800L	W5
j8ca02pqb	WR45	F775W	W5
j8ca02pcq	WR45	G800L	W5
j8ca01arq	WR45	F775W	W7
j8ca01asq	WR45	G800L	W7
j8ca01atq	WR45	F775W	W7
j8ca01auq	WR45	G800L	W7
j8caa1avq	WR45	F775W	W9
j8caa1awq	WR45	G800L	W9

FITS FILE	TARGET	ELEMENT	POINTING
j8caa1axq	WR45	F775W	W9
j8caa1ayq	WR45	G800L	W9

Table 15. The Cycle 11 INTERIM calibration observations

FITS FILE	TARGET	ELEMENT	POINTING
j8eu07qbp	WR96	F775W	W1
j8eu07qcq	WR96	G800L	W1
j8eu07qdq	WR96	F775W	W1
j8eu07qeq	WR96	G800L	W1
j8eu07q5q	WR96	F775W	W2
j8eu07q6q	WR96	G800L	W2
j8eua7qnq	WR96	F775W	W3
j8eua7qqq	WR96	G800L	W3
j8eua7qpq	WR96	F775W	W3
j8eua7qoq	WR96	G800L	W3
j8eua7qlq	WR96	F775W	W4
j8eua7qmq	WR96	G800L	W4
j8eu07q9q	WR96	F775W	W5
j8eu07qaq	WR96	G800L	W5
j8eu06ssq	WR96	F775W	Centre
j8eu06stq	WR96	G800L	Centre
j8eu06suq	WR96	F775W	Centre
j8eu06svq	WR96	G800L	Centre
j8eu06slq	WR96	F775W	W7
j8eu06soq	WR96	G800L	W7
j8eu06snq	WR96	F775W	W7
j8eu06smq	WR96	G800L	W7
j8eu06spq	WR96	F775W	W8
j8eu06srq	WR96	G800L	W8
j8eua6sxq	WR96	F775W	W9

FITS FILE	TARGET	ELEMENT	POINTING
j8eua6syq	WR96	G800L	W9
j8eua6szq	WR96	F775W	W9
j8eua6t0q	WR96	G800L	W9
j8eua6t3q	WR96	F775W	W10
j8eua6t4q	WR96	G800L	W10